Electron Paramagnetic Resonance Reveals a Large-Scale Conformational Change in the Cytoplasmic Domain of Phospholamban upon Binding to the Sarcoplasmic Reticulum Ca-ATPase†

Tara L. Kirby, Christine B. Karim, and David D. Thomas*

Department of Biochemistry, Molecular Biology and Biophysics, University of Minnesota, Minneapolis, Minnesota 55455

Received September 26, 2003; Revised Manuscript Received January 19, 2004

ABSTRACT: We used EPR spectroscopy to probe directly the interaction between phospholamban (PLB) and its regulatory target, the sarcoplasmic reticulum Ca-ATPase (SERCA). Synthetic monomeric PLB was prepared with a single cytoplasmic cysteine at residue 11, which was then spin labeled. PLB was reconstituted into membranes in the presence or absence of SERCA, and spin label mobility and accessibility were measured. The spin label was quite rotationally mobile in the absence of SERCA, but became more restricted in the presence of SERCA. SERCA also decreased the dependence of spin label mobility on PLB concentration in the membrane, indicating that SERCA reduces PLB−PLB interactions. The spin label MTSSL, attached to Cys11 on PLB by a disulfide bond, was stable at position 11 in the absence of SERCA. In the presence of SERCA, the spin label was released and a covalent bond was formed between PLB and SERCA, indicating direct interaction of one or more SERCA cysteine residues with Cys11 on PLB. The accessibility of the PLB-bound spin label IPSL to paramagnetic agents, localized in different phases of the membrane, indicates that SERCA greatly reduces the level of interaction of the spin label with the membrane surface. We propose that the cytoplasmic domain of PLB associates with the lipid surface, and that association with SERCA induces a major conformational change in PLB in which the cytoplasmic domain is drawn away from the lipid surface by SERCA.

In muscle, sequestration of calcium and its release from the sarcoplasmic reticulum (SR)[1] drive the contraction and relaxation cycle. A prime mover in this system is the SR Ca^{2+}-ATPase (SERCA) (*1*), which actively transports calcium away from the contractile proteins into the SR lumen. In heart muscle, phospholamban (PLB), a 52-residue integral membrane protein, is a critical inhibitor of SERCA, effectively reducing transfer of calcium from the cytoplasm to the SR at sub-micromolar concentrations (*2*). Upon β-adrenergic stimulation of the heart, this inhibition is relieved by phosphorylation of PLB at Ser16 by PKA and/or Thr17 by CAM-kinase (*2*−*4*).

Structural analysis of PLB is a challenge primarily because of its highly hydrophobic C-terminal domain. The amino acid sequence of PLB (*5*−*7*) suggests two major domains. The N-terminal portion of the protein (residues 1−30) is basic and contains primarily hydrophilic amino acids, as well as the two phosphorylatable residues (S16 and T17). The C-terminal portion of PLB (residues 31−52) is highly hydrophobic and determines oligomer formation (*8*). The overall secondary structure of PLB was estimated using circular dichroism (CD) and Fourier transform infrared (FTIR) spectroscopy. CD in detergent (*9*) and FTIR in lipid bilayers (*10*) both showed that PLB is 65−80% α-helical. The isolated transmembrane domain of PLB forms a stable helix (67−90%) that is approximately perpendicular to the membrane (*10*). Thus, when full-length PLB is in detergent or lipid bilayers, its cytoplasmic domain is at least partially helical. In contrast, the isolated cytoplasmic domain possesses no stable secondary structure in aqueous solution, as determined either by CD or by NMR (*11*−*13*). However, NMR spectra of the cytoplasmic domain or full-length PLB obtained in helix-promoting solvents (*14*−*16*) showed that the cytoplasmic domain is capable of producing an α-helical structure. In the absence of helix-forming solvents, the secondary structure of PLB's cytoplasmic domain, and the inhibitory function of PLB, depends on its connection with the transmembrane domain and/or its contact with detergent or lipid (*13*).

A major advance in understanding PLB structure is the recently determined NMR solution structure of monomeric PLB in detergent micelles (*17*) (Figure 1). This work indicates that there are two helical domains: one from Lys3 to Thr17 in the cytoplasmic domain and one from Gln22 to Met50 in the transmembrane domain. These two helices are connected by a four-residue semiflexible hinge that allows

† This work was supported in part by grants to D.D.T. (NIH Grant GM 27906) and C.B.K. (Grant AHA 9930083N). T.L.K. was supported by an NIH Predoctoral Training Grant in Molecular Biophysics (NIH Grant GM 08277).

* To whom correspondence should be addressed. Phone: (612) 625-0957. Fax: (612) 624-0632. E-mail: ddt@ddt.biochem.umn.edu.

[1] Abbreviations: PLB, phospholamban; SR, sarcoplasmic reticulum; SERCA, sarcoendoplasmic reticulum calcium ATPase; EPR, electron paramagnetic resonance; DOPC, 1,2-dioleoyl-*sn*-glycero-3-phosphocholine; DOPE, 1,2-dioleoyl-*sn*-glycero-3-phosphoethanolamine; IPSL, 3-(2-iodoacetamido)-PROXYL; MTSSL, 1-oxyl-2,2,5,5-tetramethyl-D3-pyrroline-3-methylmethanethiosulfonate; TPX, methylpentene polymer; NiEDDA, nickel ethylenediaminediacetic acid; DOGS−NTA−Ni(II), 1,2-dioleoyl-*sn*-glycero-3-[*N*-(5-amino-1-carboxypentyl)iminodiacetic acid)succinyl] (nickel salt); CPD, cytoplasmic domain.

10.1021/bi035749b CCC: $27.50
Published on Web 04/22/2004

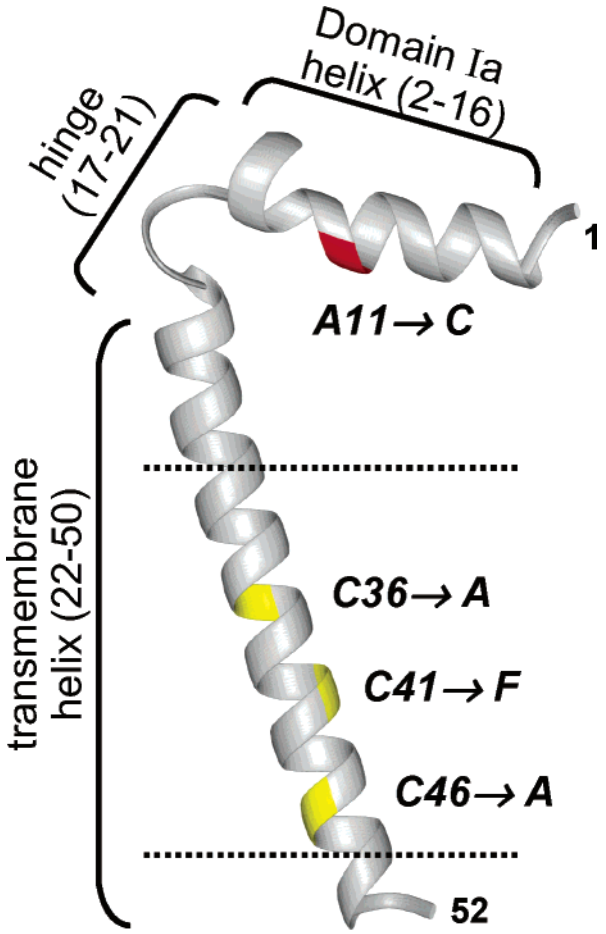

FIGURE 1: Structural model of A11C-AFA-PLB, based on the NMR structure of AFA-PLB in DPC micelles (*17*). The predicted membrane interface is represented with dashed lines. The three transmembrane Cys mutations (producing AFA-PLB) and the labeling site mutation (A11C) are denoted.

the cytoplasmic domain some freedom of movement but causes the two helical domains to be roughly perpendicular. This L-shaped conformation is consistent with solid-state NMR data on PLB in oriented lipid bilayers, indicating that the cytoplasmic domain of PLB is roughly parallel to the membrane surface, while the transmembrane domain is perpendicular (*18*). The study presented here starts from this structural model, and asks how this structure is modified by interaction with SERCA. EPR has been chosen to take this next step, because it offers capabilities that are complementary to those of NMR, particularly its superior sensitivity to structure and dynamics in large assembled systems such as membranes.

Functional interactions between SERCA and PLB are more complex than PLB's simple structure might suggest. PLB's inhibition of SERCA is relieved by the binding of Ca^{2+} to SERCA or by phosphorylation of the cytoplasmic domain of PLB. The isolated transmembrane domain of PLB inhibits SERCA just as effectively as full-length PLB does (*19*, *20*). In contrast, the isolated cytoplasmic domain has no effect on SERCA function (*19*), and neither do chimeric molecules in which the cytoplasmic domain of PLB is fused to another transmembrane sequence (*21*) or to a lipid anchor (*13*). Nevertheless, certain point mutations in residues 1−18 of the cytoplasmic domain can abolish or enhance PLB's inhibition of SERCA (*22*, *23*), indicating that structural changes in the cytoplasmic domain of PLB play an active role in the reversal of inhibition by affecting SERCA interaction. Although the cytoplasmic domain has been predicted to be α-helical, these loss-of-function mutations do not follow a clear helical pattern. Whether this indicates that the cytoplasmic domain is not helical when bound to the ATPase, or that the helix has been distorted, has not been determined (*22*, *24*, *25*).

Several points of interaction have been identified via cross-linking experiments: between residue 3 of PLB (near the N-terminus) and residues 397−402 of SERCA (*26*) and between several sites near the C-terminal end of PLB's cytoplasmic domain and various SERCA residues (*24*, *27*). Whereas the transmembrane domain shows a clear periodicity in functional effects of mutants, however, the cytoplasmic domain does not (*20*, *22*, *23*). In a cryoelectron microscopy study, Young and co-workers (*28*) co-crystallized PLB with SERCA and found areas of density that might correspond to PLB-bound SERCA. Recent modeling studies based on these and other data propose that the cytoplasmic portion of PLB unwinds upon binding to SERCA. Hutter *et al*. (*25*) predicted minimal unwinding of either the N- or C-terminal helix, with domain Ia forming multiple hydrogen bonding contacts with SERCA. More recently, using the high-resolution crystal structure of E2-thapsigargin as a starting point, Toyoshima *et al*. (*29*) proposed that the C-terminal helix unwinds before Leu31 and that the domain Ia α-helix remains relatively intact, lying in a groove in SERCA's N-domain (*24*). These proposed structural interactions must be tested directly under functional conditions using site-specific spectroscopic probes. We have chosen EPR for this next step, because it is much better suited than NMR for detection of structural dynamics in membranes.

In this study, to probe structural changes in the cytoplasmic domain of PLB upon binding of SERCA, we used the environmental sensitivity of EPR spectroscopy to detect changes in the conformation and dynamics of the cytoplasmic domain of spin-labeled PLB, both as an isolated monomer and in the SERCA-bound state. We synthesized a monomeric form of PLB (A11C-AFA-PLB) with the three native transmembrane cysteines at residues 36, 41, and 46 mutated to alanine, phenylalanine, and alanine, respectively (Figure 1). We also introduced a new cysteine at position 11 in the cytoplasmic domain, which was modified with spin labels, as described below. AFA-PLB is fully inhibitory when co-reconstituted with SERCA (*13*), and is monomeric on SDS−PAGE gels, like C46F PLB (*30*), allowing study of the PLB−SERCA interaction without confounding effects of PLB protomer−protomer interactions. A11C is positioned near the midpoint of the predicted α-helix in the cytoplasmic domain (*17*), and is near the phosphorylation sites at Ser16 and Thr17. Several residues surrounding position 11 have been shown to be important for inhibition of SERCA, although mutation of Ala11 to Val has a minimal effect on activity (*22*), suggesting that a probe at position 11 should be sensitive to the interaction of the cytoplasmic domain with SERCA without compromising the functional association between these two proteins.

We reconstituted this monomeric spin-labeled PLB with SERCA in functional lipid membranes and then used EPR to determine the effects of SERCA on the spin label's rotational dynamics and membrane topology. Both spin label

rotational dynamics, determined from analysis of the EPR spectral line shape, and accessibility to paramagnetic agents, measured by the effects of these agents in enhancing relaxation and thus decreasing saturation, were reduced in the presence of SERCA. By using paramagnetic agents localized in different portions of the sample—aqueous, intramembrane, or lipid headgroup—we demonstrated that SERCA decreased the level of interaction of the spin label with lipid headgroups more than with aqueous or intramembrane agents. Additionally, in the presence of SERCA, we observed increased spin probe lability, as well as disulfide cross-linking between PLBs and SERCA-bound PLB, indicating direct interaction between one or more SERCA cysteine residues and Cys11 on PLB. We conclude that binding of SERCA induces a major conformational change in the region around residue 11 of PLB, consistent with a model in which the cytoplasmic domain of PLB is drawn away from the lipid surface by SERCA.

MATERIALS AND METHODS

Synthesis of A11C-AFA-PLB. The general method of the PLB solid-phase peptide synthesis was essentially as described previously (*31*). Starting with Fmoc-Leu-PEG-PS resin (0.2 mmol/g), automated AC11C-AFA-PLB chain assembly was carried out with a PE Biosystems Pioneer peptide synthesis system. All couplings were in NMP, as mediated by HBTU/HOBt/DIEA (4:4:8 eq. with respect to peptide resin). Fmoc removal was achieved with 20% piperidine and 2% DBU in NMP. The final deprotection and cleavage were carried out with Reagent K (82.5% trifluoroacetic acid, 5% phenol, 5% thioanisole, 2.5% 1,2-ethanedithiol, and 5% water) for 4 h at 25 °C. The mixture was filtered, and the resin was washed with 2 mL of freshly prepared Reagent K. The combined filtrates were concentrated under N_2, and precipitated in 30 mL of diethyl ether at 0 °C. The precipitated peptide was collected by centrifugation and washed three times with 30 mL of cold diethyl ether. The crude peptide was dissolved in 5 mL of 70% TFA and purified by HPLC on a C-18 column (Vydac, 218TP54, 5 μm, 300 Å, 4.6 mm × 250 mm) that had been equilibrated with 95% water, 2% acetonitrile, and 3% 2-propanol. Peptide elution was achieved with a linear gradient to a final solvent composition of 5% water, 38% acetonitrile, and 57% 2-propanol. Fractions containing peptide were lyophilized to yield 37 mg of A11C-AFA-PLB (15% yield based on starting resin).

Peptide Analysis by Mass Spectrometry. Mass spectra were acquired with a Bruker Biflex III matrix-assisted laser desorption ionization time-of-flight (MALDI-TOF) system, which is equipped with an N_2 laser (337 nm, pulse length of 3 ns) and a microchannel plate detector. Samples were co-crystallized with the matrix 3,5-dimethoxy-4-hydroxycinnamic acid (sinapinic acid), and the data were collected in the linear mode, positive polarity, with an accelerating potential of 19 kV. Each spectrum is the accumulation of 100−400 laser shots.

SDS−PAGE. Proteins were electrophoresed on a 10 to 20% Tris-Tricine Ready Gel (Bio-Rad Laboratories, Hercules, CA) at a constant voltage of 80 V. For visualization of proteins, the gel was stained with Coomassie blue R-250 (Sigma-Aldrich, St. Louis, MO). Protein amounts on Coomassie blue-stained gels and Western blots were quantitated by gel densitometry using the Bio-Rad model GS-700 imaging densitometer and Molecular Analyst software, and compared with standards of known concentrations.

Circular Dichroism. The method for determination of the secondary structure of PLB by CD was previously described (*13*). CD spectra were recorded on a Jasco (Easton, MD) J-710 spectrophotometer at 25 °C using a 0.01 cm path length quartz cuvette. Acquisition was performed using a scan rate of 50 nm/min, a bandwidth of 1 nm, and a response time of 2 s. The corresponding baseline [10 mM Tris (pH 7.0), 0.2% $C_{12}E_8$ buffer] was subtracted from each spectrum. Reported spectra are averages of six scans and are expressed as mean residue ellipticity, [θ]. Aqueous solutions for CD were prepared by drying a volume of the peptide stock solution (~3 mg/mL in chloroform or methanol) under a low-level flow of N_2 and adding the appropriate amount of buffer to give final peptide concentrations of 0.1−0.5 mM. Linear combinations of α-helix and random coil basis spectra were used to estimate secondary structure contributions from fits to experimental CD spectra.

Co-Reconstitution of the Ca-ATPase/PLB Vesicles. SR vesicles for PLB−Ca-ATPase interaction studies were prepared from the fast-twitch skeletal muscle of New Zealand white rabbits (*32*). The Ca-ATPase from the SR vesicles was purified using a reactive-red affinity column essentially the same as that described previously (*33*), except that dithiothreitol was omitted from the elution buffer protein. The method used for the functional reconstitution of Ca-ATPase with PLB has been described previously (*19*). In short, 22 μg of PLB was solubilized in 20 μL of chloroform containing 0.2 mg of lipids (4:1 DOPC/DOPE mixture). The solvent was evaporated to dryness, and the dried film of the lipid and PLB was hydrated with 80 μL of 25 mM imidazole (pH 7.0) by vortexing followed by brief sonication. The resulting vesicles were diluted to 20 mM imidazole (pH 7.0), 0.1 M KCl, 5 mM $MgCl_2$, and 10% glycerol; 0.4 mg of $C_{12}E_8$ (Calbiochem, San Diego, CA) was added, followed by 40 mg of purified Ca-ATPase. The final volume was adjusted to 200 μL with buffer. The detergent was removed by incubation with 20 mg of hydrated Biobeads (BioRad) for 3 h at room temperature. The Ca-ATPase/PLB lipid vesicles were separated from Biobeads and assayed immediately. All Ca-ATPase/PLB co-reconstitutions for functional assays used a fixed molar ratio of 10 PLB/Ca-ATPase (*34*, *35*).

ATPase Activity Measurements. Ca-ATPase activity was measured using an enzyme-linked assay (*36*), performed in microtiter plate wells as described previously (*37*). The assay was carried out in triplicate at each of 12 different free calcium concentrations in a volume of 175 μL. Each well contained 1−3 μg of Ca-ATPase (5−15 μL of vesicles), 50 mM imidazole (pH 7.0), 0.1 M KCl, 5 mM $MgCl_2$, 0.5 mM EGTA, 0.5 mM phosphoenolpyruvate, 2.5 mM ATP, 0.2 mM NADH, 2 IU of pyruvate kinase, 2 IU of lactate dehydrogenase, and 1−2 μg of calcium ionophore (A23187, Sigma-Aldrich). The absorbance of NADH was monitored at 340 nm (extinction coefficient of 6.22×10^3 M^{-1} cm^{-1}, path length of 0.55 cm) to determine the rate of ATP hydrolysis. The assays were performed at 25 °C in a Thermomax microplate reader (Molecular Devices, Sunnyvale, CA).

Preparation of Spin-Labeled PLB. We labeled A11C-AFA-PLB with a cysteine-reactive spin label probe, either

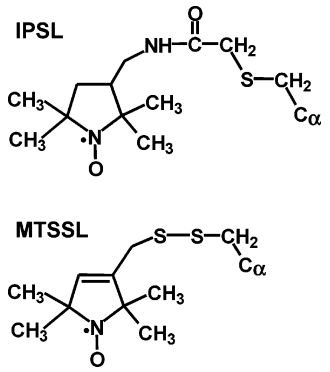

FIGURE 2: Spin label probes, showing the linkage to cysteine.

IPSL [3-(2-iodoacetamido)-PROXYL, Sigma-Aldrich] or MTSSL (1-oxyl-2,2,5,5-tetramethyl-D3-pyrroline-3-methyl methanethiosulfonate, Toronto Research Chemicals, North York, ON) (Figure 2). Both probes form a covalent bond with the sulfide moiety on the cysteine residue; the disulfide formed by reaction with MTSSL is reversible under reducing conditions, while the iodoacetimide of IPSL forms a more stable linkage. The probes are similar in structure, with the nitroxide incorporated into a five-membered ring, although the double bond and shorter linkage of MTSSL make it less flexible, more compact, and more sensitive to the motion of the protein backbone, so it is the probe of choice for most recent site-directed spin labeling studies (*38*).

To label peptide with MTSSL, synthetic PLB was dissolved in 60 mM Tris-HCl and 0.1% SDS (pH 7.5) at a concentration of 1−2 mg/mL. A 10-fold molar excess of MTSSL was added from a 50 mM stock solution in DMF, and the sample was incubated in the dark for 16 h at 4 °C. To label the peptide with IPSL, synthetic A11C-AFA-PLB was dissolved in 60 mM Tris-HCl and 0.1% SDS (pH 8.0) at a concentration of 1−2 mg/mL. A 10-fold molar excess of IPSL was added from a 50 mM stock solution in DMF, and the sample was incubated in the dark for 24−36 h at 4 °C.

Free spin label was removed from the peptide by HPLC using a diphenyl column (Vydac, 219TP510, 5 μm, 300 Å, 10 mm × 250 mm). Protein was eluted using a 30 min, 0 to 100% A to B gradient with a flow rate of 2.5 mL/min. Buffer A consisted of 95% H_2O, 2% acetonitrile, 3% 2-propanol, and 0.1% trifluoroacetic acid. Buffer B consisted of 5% H_2O, 38% acetonitrile, 57% 2-propanol, and 0.1% trifluoroacetic acid. The elution time for PLB was approximately 22−25 min. The eluted protein was lyophilized and dissolved in methanol at a concentration of 1−2 mg/mL.

Reconstitution of PLB and SERCA for EPR Experiments. PLB in methanol was mixed with lipid, and the mixture was dried under N_2. Traces of solvent were removed by desiccation. For PLB-only reconstitution, vesicles were resuspended in 20 mM MOPS (pH 7.0) unless otherwise noted, and sonicated for 30 s. For SERCA-bound PLB, vesicles were resuspended in a final concentration of 20 mM MOPS (pH 7.0), 0.1 M NaCl, 5 mM $MgCl_2$, and 10% glycerol, unless otherwise noted. Vesicles were sonicated, and then SERCA was added and the mixture stirred gently. $C_{12}E_8$ was added to a final concentration of 2 mg/mL, and the mixture was stirred gently for 5−10 min to allow solubilization of vesicles. The detergent was removed by incubation with Biobeads (50 mg/mg of detergent) for 3 h at room temperature. For both PLB-only and PLB−SERCA samples, samples were diluted to 3 mL in original resuspension buffer and pelleted in a TLA-100.3 Beckman rotor at 100 000 rpm for 30 min at 4 °C. The sample was resuspended in a total volume of 20 μL of the original buffer and then sonicated for 30 s.

EPR Data Acquisition. Spectra were acquired using a Bruker EleXsys 500 spectrometer equipped with the SHQ cavity. Spectra were acquired over a range of 120 G at varying microwave powers. For all spectra, field modulation was at a frequency of 100 kHz with a peak-to-peak amplitude of 2.0 G. Except for saturation experiments, all spectra were recorded at a microwave power sufficiently low to ensure the absence of saturation. The sample temperature was maintained at 25 °C using the standard Bruker temperature controller, with the sample contained inside a quartz dewar, through which gas was passed after being cooled in a dry ice/2-propanol bath and passed through a heater sensor. Typically, samples containing 8.25 nmol (50 μg) of PLB in lipid, and other components, were resuspended in 20 μL of buffer. Five microliters of sample was loaded into a 0.6 mm inside diameter TPX loop-gap resonator capillary (Medical Advances, Milwaukee, WI), with a total sample length of approximately 10 mm. The sample was centered in the active part of the cavity. All samples for saturation experiments were flushed with N_2 gas or with zero-grade air, as appropriate.

Analysis of Spin-Label Rotational Dynamics. Simulations of EPR spectra and fits to experimental spectra were carried out using the program NLSL (*39*). Experimental spectra were fit to simulated spectra containing one or two populations (spectral components). Simulations assumed the MOMD model, which assumes that the membrane surfaces are randomly oriented, and all detectable (sub-microsecond) rotational motion occurs relative to the membrane. For each population, it was assumed that rotational motion is characterized by a single mode of motion, characterized by a rotational correlation time τ_R and an order parameter S. Rigid-limit values for magnetic interaction tensors were determined from spectra obtained at −60 °C, and isotropic values were obtained from the free spin label in solution at 25 °C. For each component, the order parameter S, the correlation time, and the mole fraction of that population were determined from the best-fit simulation. The best fit was determined by minimizing χ^2. The uncertainty for each parameter was estimated from the range of values obtained by (a) starting the fits from a wide range of initial values and (b) fitting spectra obtained from several different samples. To obtain a more intuitive interpretation of the order parameter, the motion was modeled as a wobble-in cone with an angular amplitude θ_c (half-cone angle) given by

$$\theta_c = \cos^{-1}\left[\frac{(1 + 8S)^{0.5} - 1}{2}\right] \quad (1)$$

where S values of 1, 0.5, and 0 correspond to θ_c values of 0°, 52°, and 90°, respectively. This describes the amplitude of rotational motion of the spin label with the correlation time τ_R. This order parameter reflects both peptide backbone flexibility and motions of the spin label relative to the backbone. However, experiments with well-defined model systems and comparison with NMR data have shown that

an order parameter of <0.5 implies substantial backbone flexibility, inconsistent with an ordered α-helix (*38*).

EPR Accessibility Studies. Accessibility of the spin label to paramagnetic agents was determined from enhancement of spin label relaxation. Agents were chosen to probe accessibility to different phases of the sample. NiEDDA [prepared as described previously (*40*)] was used to probe accessibility to the aqueous phase. A Ni ion chelated by a lipid headgroup [DOGS−NTA−Ni(II), Avanti Polar Lipids, Alabaster, AL] was chosen to probe accessibility to the membrane interface. Zero-grade air was used to probe accessibility to oxygen, in both the aqueous and lipid phases. These reagents are all collisional *quenchers*, in the sense that they enhance spin relaxation and thus decrease saturation, returning the system toward Boltzmann equilibrium (*41*). Decreased saturation was detected by increasing the intensity of the exciting microwave radiation to a saturating level and then adding the paramagnetic quencher and measuring how much more power was required to cause saturation. In this "saturation rollover" experiment, the signal intensity was recorded as a function of incident microwave power, and the data set was fit to

$$A = I\left[1 + \frac{(2^{1/\epsilon} - 1)P}{P_{1/2}}\right]^{-\epsilon} \quad (2)$$

where A is the signal intensity, P is the incident microwave power, $P_{1/2}$ is the microwave power at half-saturation, and ϵ is a measure of the homogeneity of the saturation line (*40*). In the nonlinear least-squares fit, $P_{1/2}$ was allowed to vary freely and ϵ was allowed to vary in the range of 0.5−1.5. $\Delta P_{1/2}$, the increase in $P_{1/2}$ due to quencher, is proportional to the collision frequency, which is proportional to the quencher concentration, accessibility, and fluidity. Therefore, at a constant quencher concentration and fluidity, $\Delta P_{1/2}$ is simply proportional to accessibility. The collision frequency W (and the accessibility) of the spin label with the paramagnetic quencher is related to $\Delta P_{1/2}$ by

$$W \propto \Delta P_{1/2} T_2 = \Delta P_{1/2}/\Delta H_0 = \Delta P'_{1/2} \quad (3)$$

where W_x is the collision frequency and T_2 is the spin−spin relaxation time, assuming that T_2 is not significantly changed by the presence of the quencher (*42*). Spectral parameters for saturation data were determined using an analysis program written for Mathematica 4 (Wolfram Research, Champaign, IL), and were fit to eq 2 using NonLinear Curve Fit in Origin, version 6.0.

The effect of SERCA on accessibility for each quencher was compared using the fractional accessibility, F, defined as

$$F = \frac{\Delta P'_{1/2}(+\text{SERCA})}{\Delta P'_{1/2}(-\text{SERCA})} \quad (4)$$

where +SERCA represents the sample containing both PLB and SERCA and −SERCA the sample containing PLB alone.

RESULTS

Characterization of Synthetic A11C-AFA-PLB. HPLC and SDS−PAGE both indicated that the synthesized and purified compound was extremely pure. The mass was verified by MALDI-TOF mass spectrometry (Figure 3). The *m*/*z* ratio (M + H) of the principal peak was 6092.0, which corresponds well with the predicted value of 6092.6. Amino acid analysis confirmed the peptide had the correct composition. We compared the secondary structures of AFA-PLB, A11C-AFA-PLB, and spin-labeled A11C-AFA-PLB by CD (Figure 4). The spectra of AFA-PLB and A11C-AFA-PLB were essentially identical, characterized by a minimum at 209 nm and a maximum at 222 nm. Analysis of these spectra, as linear combinations of basis spectra, indicates a predominantly α-helical secondary structure (85−90%), as previously reported for AFA-PLB (*13*). Labeling with IPSL (data not shown) or MTSSL (Figure 4) did not significantly affect the secondary structure.

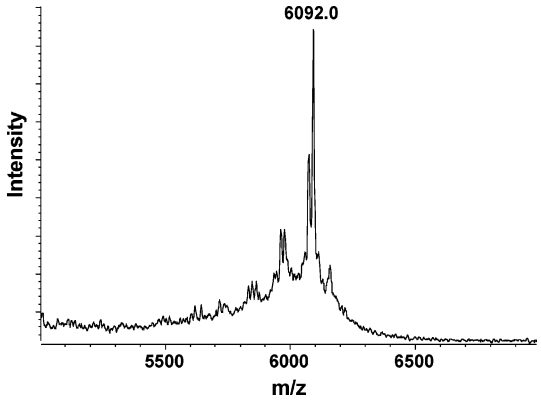

FIGURE 3: MALDI-TOF mass spectrometry of A11C-AFA-PLB.

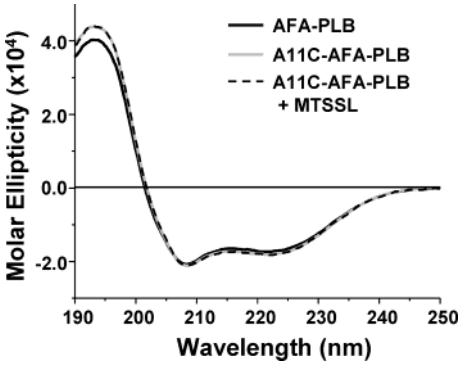

FIGURE 4: Circular dichroism of PLB mutants in 10 mM Tris and 0.2% $C_{12}E_8$ (pH 7.0).

The functional effects of labeled and unlabeled A11C-AFA-PLB peptides were studied by measuring their effects on calcium-dependent ATPase activity (Figure 5). PLB was reconstituted at a 10-fold molar excess over SERCA, at a 700:1 lipid:SERCA molar ratio. As shown in Figure 5, AFA-PLB shifts the pK_{Ca} for SERCA (the pCa at which ATPase activity is half-maximal) by 0.32 ± 0.05, which is comparable to previous measurements, and confirms that AFA-PLB has an inhibitory function similar to that of wild-type PLB (*13*). Mutation of Ala11 to Cys decreases the activity slightly but not significantly, with a pK_{Ca} shift of 0.25 ± 0.06 (not shown). This is consistent with a previous report that mutation of Ala11 to Val only slightly decreases inhibition of SERCA by wild-type PLB (*22*). The addition of either spin label also had no significant effect on the activity of A11C-AFA-PLB (data shown for IPSL).

Mutagenesis of cysteines in the transmembrane domain to Ser, Ala, or Phe destabilizes the PLB oligomer, and

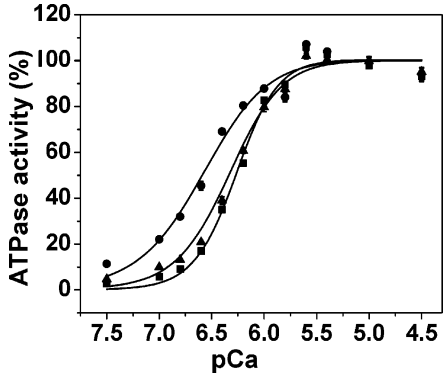

FIGURE 5: ATPase activity as a function of Ca^{2+} concentration, normalized to maximal activity, showing control (no PLB) (●), AFA-PLB (■), and IPSL−A11C-AFA-PLB (▲).

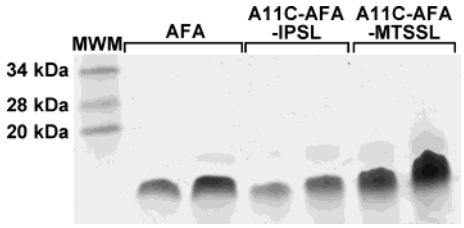

FIGURE 6: SDS−PAGE of AFA-PLB and labeled mutants.

mutation of Cys41 to Phe renders PLB monomeric on SDS−PAGE (*30*). AFA-PLB is also predominantly monomeric on SDS−PAGE (Figure 6). Introduction of a spin-labeled cysteine at residue 11 of AFA-PLB does not affect the oligomeric stability in SDS; AFA and spin-labeled A11C-AFA-PLB are 95% monomeric as determined by gel densitometry. It has previously been shown that the oligomeric state of a PLB analogue in SDS−PAGE is a good indicator of its oligomeric state in lipid bilayers (*43*, *44*).

EPR Spectra of Spin-Labeled A11C-AFA-PLB. For the PLB-only samples, MTSSL-labeled A11C-AFA-PLB (MTSSL−PLB) and IPSL-labeled A11C-AFA-PLB (IPSL−PLB) were reconstituted into lipids at a ratio of 100 lipids/PLB; where SERCA was present, the co-reconstitution was carried out at a ratio of 150 lipids/PLB and 1 PLB/SERCA. Decreasing the ratio to 0.5 PLB/SERCA had no effect on the results, indicating saturation of PLB binding by SERCA. Spectra are presented in Figure 7. In the absence of SERCA, the spectra are dominated by a narrow component indicating weakly-immobilized spin labels. Rotational dynamic was analyzed as described in Materials and Methods and summarized in Table 1. Data are given for IPSL at two different lipid:PLB ratios, as discussed below. In all cases except for MTSSL, two components gave a better fit than one. For IPSL−PLB, a minor population (25%) is weakly immobilized, with a short correlation time ($\tau_{R1} = 0.63$ ns) and a large amplitude ($\theta_c = 86°$, from $S = 0.04$), while the major population (75%) is moderately immobilized ($\tau_{R1} = 4.2$ ns and $\theta_c = 56°$). For MTSSL−PLB, the single component has intermediate mobility ($\tau_R = 2.6$ ns and $\theta_c = 77°$). For both spin labels, the order parameters of the mobile components are lower than expected for these spin labels attached to Cys on the surface of a rigid α-helix (*38*, *45*).

Upon addition of SERCA, each spectrum broadens considerably and a strongly immobilized component becomes evident from the resolved peaks in the wings of the spectrum. The order parameter S for the strongly immobilized component is similar for the two samples, 0.89 for IPSL−PLB and 0.92 for MTSSL−PLB, with θ_c values of 22° and 19°, respectively, and the correlation times are much longer than those observed in the absence of SERCA (Table 1). This restriction of motion suggests increased helical stability and/or direct steric interaction with SERCA. For both spin labels, the mobile component becomes slightly slower (longer τ_R) but its order parameter does not change significantly.

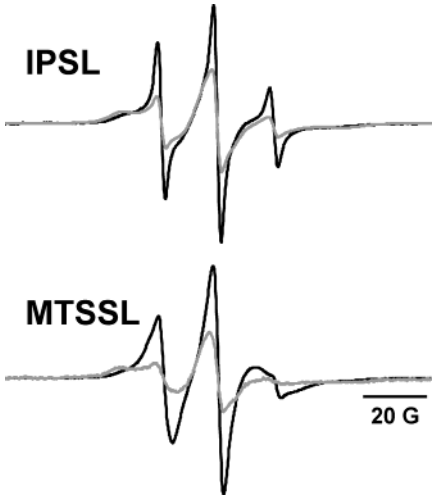

FIGURE 7: EPR spectra of A11C-AFA-PLB, labeled at Cys11 with the indicated spin label, without (black) or with (gray) SERCA.

Accessibility of IPSL−PLB to Paramagnetic Agents. To further investigate the conformational difference between the SERCA-bound and unbound PLB cytoplasmic domains, we measured the accessibility of IPSL−PLB to paramagnetic relaxation agents (quenchers) that are localized differently within the membrane sample, to obtain more detailed insight into the location of the labeled site with respect to the membrane surface, and to determine the effect of SERCA on this location. We used oxygen (zero-grade air), which partitions 90:10 between the membrane and aqueous fractions; 20 mM NiEDDA, a hydrophilic aqueous agent; and DOGS−NTA−Ni(II) (1 per 21 lipids), which contains nickel bound to the lipid headgroup. IPSL−PLB was reconstituted at a ratio of 500 lipids per PLB. EPR spectra were measured at a constant temperature (25 °C) over a range of incident microwave power. To determine the half-saturation point, $P_{1/2}$, the data were fit to eq 2. The saturation curves, shown as normalized signal intensity ($S/P^{0.5}$) versus power, are shown in Figure 8.

To quantitate the effect of SERCA, we calculated the fractional accessibility F (eq 4), which is the ratio of $\Delta P'_{1/2}$ for PLB and SERCA to $\Delta P'_{1/2}$ for PLB alone. Figure 9 shows that $F < 1$ for all three quenchers, indicating that SERCA decreases the accessibility of the spin-labeled site. The most likely interpretation is that the labeled site on PLB (position 11 on the cytoplasmic domain) interacts directly with SERCA.

Further insight was obtained from comparing the relative effects of SERCA on the three different paramagnetic agents. SERCA has its largest effect ($F = 0.13 \pm 0.01$) on accessibility to DOGS−NTA−Ni(II) (completely constrained to the membrane surface) and its smallest effect ($F = 0.50 \pm 0.04$) on accessibility to NiEDDA (completely localized in the aqueous phase), with an intermediate value ($F = 0.34 \pm 0.03$) observed for oxygen (partitions between both

Table 1: Spin Label Dynamics[a]

	X_1	S_1	θ_{c1} (deg)	τ_{R1} (ns)	S_2	θ_{c2} (deg)	τ_{R2} (ns)
IPSL (100 L/P)	0.25 (0.01)	0.04 (0.02)	86 (2)	0.63 (0.05)	0.44 (0.02)	56 (2)	4.2 (0.5)
IPSL (500 L/P)	0.31 (0.02)	0.04 (0.02)	86 (2)	0.62 (0.04)	0.44 (0.03)	56 (3)	4.2 (0.8)
MTSSL	1.00 (0.01)	0.14 (0.04)	77 (3)	2.6 (0.2)	–	–	–
IPSL and SERCA	0.13 (0.01)	0.05 (0.03)	85 (3)	1.0 (0.3)	0.89 (0.04)	22 (4)	33 (5)
MTSSL and SERCA	0.42 (0.02)	0.14 (0.06)	77 (5)	2.6 (0.4)	0.92 (0.05)	19 (7)	17 (3)

[a] Parameters were obtained from analysis of EPR spectra with NLSL as described in Materials and Methods. X_1 is the mole fraction of component 1. S is the order parameter. θ_c is the cone angle derived from S (eq 1). τ_R is the rotational correlation time. Estimated errors are in parentheses.

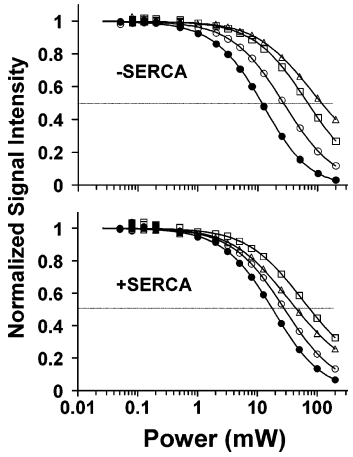

FIGURE 8: Normalized saturation curves for IPSL−PLB, without (top) or with (bottom) SERCA: (●) N_2, (○) O_2, (□) NiEDDA, and (△) Ni^{2+} chelated to the lipid headgroup.

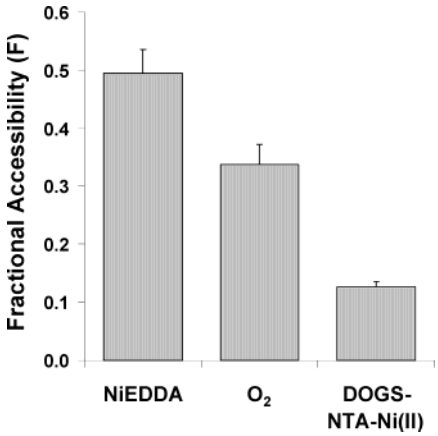

FIGURE 9: Accessibility of IPSL−PLB in the presence of SERCA, calculated from the data in Figure 8. F is the collision accessibility in the presence of SERCA relative to that in the absence of SERCA (eq 4).

phases). For DOGS−NTA−Ni(II) to collide with IPSL at position 11, this region of the cytoplasmic domain must spend considerable time at or near (within 14 Å) the membrane surface (*46*). We conclude that SERCA moderately decreases the spin label's exposure to the aqueous phase, probably due to direct contact of the PLB cytoplasmic domain with SERCA, and that SERCA moves the cytoplasmic domain of PLB away from the membrane surface.

Lipid Concentration Affects Line Shape Only in the Absence of SERCA. To determine the sensitivity of the EPR line shape to lipid concentration, we compared membrane samples containing IPSL−PLB or IPSL−PLB with SERCA, at two lipid concentrations. The more concentrated sample contained 100 lipids/PLB for IPSL−PLB and 150 lipids/PLB for IPSL−PLB with SERCA (to accommodate the

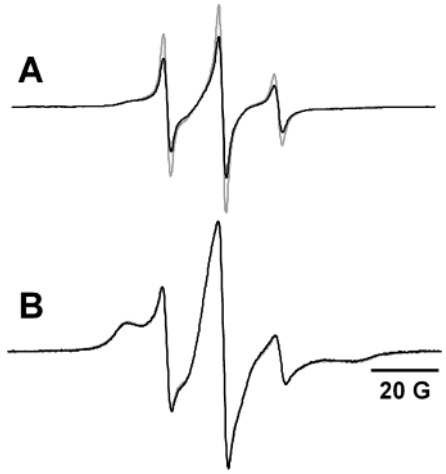

FIGURE 10: Effect of lipid concentration on EPR line shape. (A) PLB only, at 500 lipids/PLB (gray) and 100 lipids/PLB (black). (B) PLB with SERCA, at 500 lipids/PLB (gray) and 150 lipids/PLB (black). Paris of spectra are normalized to a double integral, so the intensity decrease due to the lower lipid content in panel A reflects decreased mobility.

increased volume of SERCA in the lipid bilayer). The more diluted sample contained 500 lipids/PLB for both IPSL−PLB and IPSL−PLB with SERCA. In the absence of SERCA (Figure 10A), dilution increased the more mobile population from 25 ± 2 to 31 ± 1%, without significantly affecting the dynamics of either population (Table 1). In the presence of SERCA (Figure 10B), dilution had no significant effect on the EPR spectrum. We repeated the experiments depicted in Figure 10A with PLB that was only 25% spin labeled, and observed the same results. This shows that the effect of lipid dilution was due to a change in spin label dynamics, not to a decrease in the level of spin−spin interaction.

Disulfide Interchange Occurs Only in the Presence of SERCA. The first spin label probe we used to label A11C-AFA-PLB was MTSSL. We have used this probe successfully in our previous experiments with PLB (*47*), and it has been the probe of choice for many site-directed spin labeling studies (*48*). MTSSL attaches to a protein by forming a disulfide bond with cysteine (Figure 2). While the spectrum of MTSSL−PLB alone was quite stable, the addition of SERCA caused the appearance of a highly mobile spectral component (Figure 11A), corresponding to free spin label. The presence of SERCA destabilizes the disulfide linkage between MTSSL and PLB, with a first-order rate constant of 0.45 s^{-1} at 25 °C, which was observed by monitoring the appearance of the narrow spectrum corresponding to free spin label. This effect was observed in the absence of reductants such as DTT. A Western blot of the sample using an anti-PLB monoclonal antibody revealed that, in addition

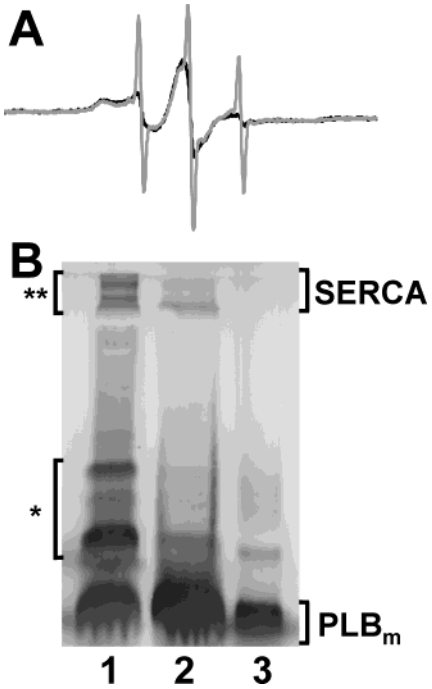

FIGURE 11: (A) EPR spectra of MTSSL−PLB with SERCA, before (black) and after (gray) a 3 h incubation at 25 °C. (B) Anti-PLB Western blot of the EPR sample. The electrophoretic mobilities of SERCA and PLB monomer on the corresponding Coomassie-stained gel are given: lane 1, untreated sample; lane 2, sample treated with 10% β-mercaptoethanol; and lane 3, AFA-PLB standard. One asterisk indicates the PLB aggregates; two asterisks indicate the PLB-SERCA complex.

to the expected monomeric PLB band, there were also several higher-molecular weight bands present in the sample (Figure 11B), probably corresponding to PLB−PLB dimers and higher-order aggregates (Figure 11B, one asterisk) and a PLB−SERCA complex (Figure 11B, two asterisks). The magnitudes of these bands were greatly reduced upon addition of 10% β-mercaptoethanol to the sample loading buffer, indicating that they corresponded to disulfide-linked proteins. The most likely interpretation is that one or more Cys residues of SERCA participate in disulfide exchange with MTSSL−PLB, resulting in SERCA−PLB and PLB−PLB disulfide bonds, which are described by

$$R1-S-S-R2 + R3-S^- \leftrightarrow R1-S-S-R3 + R2-S^-$$

where R1−S−S−R2 represents MTSSL−PLB (Figure 2) and R3−S$^-$ represents SERCA or another PLB with a reactive cysteine. This phenomenon does not occur with MTSSL-labeled transmembrane mutants of PLB in the presence of SERCA (data not shown).

DISCUSSION

Our results provide evidence for a major conformational change in the cytoplasmic domain of PLB upon binding to SERCA. Solid-state NMR studies in lipid (*18*) and solution NMR studies in lipid-mimicking detergent micelles (*17*) or organic mixtures (*15*, *16*) suggest that monomeric PLB forms a "7-shaped" structure in membranes. Perturbation of NMR signals by lipid spin labels provided evidence that cytoplasmic domain Ia interacts closely with the micellar interface (*17*). The NMR experiments were performed in detergent micelles at 50 °C and pH 4, in the absence of SERCA, so it is important to test this result in lipid membranes under more physiological conditions and to determine the effects of SERCA. Models of the PLB−SERCA interaction indicate that the N-terminus of PLB binds to SERCA at a point significantly far from the membrane interface, estimated to be 45−50 Å (*24*, *25*). Taken together with the solution structure of PLB and these modeling results, our data are consistent with the model shown in Figure 12. The isolated monomeric PLB forms a 7-shaped structure in the membrane (Figure 1), with the transmembrane domain approximately perpendicular to the membrane and cytoplasmic domain Ia interacting dynamically with the membrane surface (Figure 12A). This cytoplasmic domain shows considerable nanosecond dynamics, so it may have both ordered (Figure 12A) and dynamically disordered conformations (Figure 12B). Upon SERCA binding, the cytoplasmic domain moves up and away from the membrane surface, forming an ordered complex with SERCA (Figure 12D).

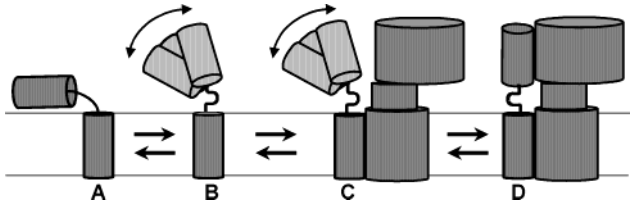

FIGURE 12: Model for the conformation of the PLB cytoplasmic domain (CPD). In the absence of SERCA (left), the CPD interacts dynamically with the lipid surface (A), including a substantial disordered population (B). When PLB binds to SERCA (C), the equilibrium is shifted toward a strongly bound and ordered form of the CPD that is removed from contact with the lipid surface (D). This complex stabilizes an inhibited conformation of SERCA.

Interpretation of Spin Label Dynamics. EPR spectra of IPSL−PLB (Figure 7) show evidence for two modes of dynamics in cytoplasmic domain Ia (Table 1), consistent with the presence of ordered (Figure 12A) and dynamically disordered (Figure 12B) modes of PLB dynamics. These may represent two separate populations or two conformations of each PLB molecule; we can only say that these two conformations are not exchanging on the sub-microsecond time scale. The lack of two resolved components for MTSSL is probably due to dynamics of this probe relative to the protein (*45*). EPR data clearly show partial immobilization of the spin label at position 11 for both spin labels upon binding of SERCA (Figure 7), as reported previously for EPR or fluorescent probes near the N-terminus of PLB (*49*). Remarkably, although the mobilities of the two spin labels differ in unbound PLB, addition of SERCA results in a similar degree of immobilization in both cases. In both cases, a portion of the spin label population remains at approximately the same mobility as that for unbound PLB. Our two-component analysis of the EPR spectrum indicates that this mobile component comprises 13 ± 2% of the spectrum of IPSL−PLB with SERCA. If the more restricted population represents the cytoplasmic domain of PLB bound to SERCA, then the weakly immobilized fraction can be assigned to PLB, whose cytoplasmic domain is not in contact with SERCA, either because the cytoplasmic domain itself is free (Figure 12C) or because the entire PLB molecule is dissociated from SERCA (Figure 12D). An alternative explanation (not shown) would be that the spin-labeled cytoplasmic domain has two conformations when bound to SERCA.

Accessibility data (Figure 9) also support the model in Figure 12. Accessibility (collision frequency) was reduced significantly for the freely diffusible quenchers (NiEDDA and oxygen) by the addition of SERCA, and was nearly abolished for DOGS−NTA−Ni(II), which is localized in the membrane interface. The reduction in accessibility to NiEDDA suggests occlusion of the spin label by SERCA. Since most of the oxygen (90%) partitions into the membrane, the reduced fractional accessibility to oxygen (32%) compared to the accessibility to NiEDDA (49%) suggests a reduction in the number of collisions with the membrane. The strongest evidence for this conclusion arises from the dramatic reduction (from 100 to 13% upon addition of SERCA) in accessibility for the membrane interface-localized DOGS−NTA−Ni(II). This corresponds well with the 13% mobile component observed in the EPR spectrum of IPSL−PLB with SERCA, so the accessibility to DOGS−NTA−Ni(II) may also reflect these two populations. Because Ni is confined to a 14 Å slice on the aqueous side of the membrane interface in DOGS−NTA−Ni(II) (*46*), cytoplasmic domain Ia must move a significant distance away from the membrane interface upon SERCA binding, with little or no contact in the SERCA-bound state.

Effects of Lipid Concentration on Line Shape. In the absence of SERCA, the EPR spectra exhibited more restriction at higher PLB:lipid ratios, but this effect was abolished by SERCA (Figure 10). This result is consistent with the model proposed above (Figure 12). If PLB's cytoplasmic domain lies on the membrane surface, then a high PLB:lipid ratio should cause crowding and thus restrict probe mobility, as observed. If SERCA binds PLB and raises it to a vertical orientation, PLB−PLB interactions should be diminished, thus eliminating the concentration effect, as observed.

MTSSL Disulfide Interchange. Our observations indicate that the MTSSL disulfide bond is quite stable until SERCA is allowed to interact with PLB, causing the spin label to be released and simultaneously inducing bonds (presumably disulfide) between PLB and SERCA, or between PLB and PLB. The formation of a disulfide bond with SERCA is interesting in light of two recent reports: the first showing that another PLB mutant, N30C-PLB, can cross-link with Cys318 on SERCA (*27*) and the second showing that N27C in PLB forms a disulfide bond with the L321C SERCA mutant, and V49C in PLB forms a disulfide bond with the V89C SERCA mutant (*24*). To investigate whether A11C-PLB also cross-links with a specific cysteine on SERCA, it will be necessary to analyze tryptic digests of the PLB−SERCA homodimer by peptide sequencing to determine the identity of the reactive cysteine on SERCA. It will also be important to test other cytoplasmic domain cysteine mutants of PLB for similar behavior in the presence of SERCA.

Dynamic Equilibrium between an Ordered and a Disordered Cytoplasmic Helix. The observation of two components in the spectra of both PLB and PLB with SERCA probably reflects two structural states of the PLB protein backbone (ordered and disordered) in the vicinity of the spin label. While spin label mobility can reflect motions of the spin label relative to the protein backbone, it has been shown that the spin label MTSSL bound to a rigid α-helix consistently has an order parameter of ≥ 0.5 (*38*). Since both spin labels exhibit order parameters much lower than 0.5 when bound to SERCA-free PLB (Table 1), it is likely that the helix of cytoplasmic domain Ia is at least partially disordered (Figure 12B). This hypothesis is also supported by NMR hydrogen exchange data from PLB in detergent micelles, which show that the cytoplasmic helix is much more dynamic than the transmembrane domain (*17*). Taken together, our mobility and accessibility data suggest that the cytoplasmic helix of PLB has two intrinsic conformations, one more ordered than the other, and that the more ordered conformation is stabilized by interaction with SERCA.

The role of the order−disorder equilibrium in the domain Ia helix may have important implications for the mechanism of interaction of the cytoplasmic domain of PLB with SERCA. Other studies have shown a change in structural order in cytoplasmic domain Ib upon SERCA binding. Experiments with a monomeric PLB mutant fluorescently labeled at A24C showed that addition of SERCA increased the solvent exposure of the label, as well as the rate of local probe motion (*50*). A contradictory result, obtained by solid-state NMR of monomeric PLB, suggested not only that residues 21−24 remain helical upon addition of SERCA but also that association with SERCA induces helical structure between residues 24 and 26 (*51*). Clearly, investigating the relationship between the structural dynamics of PLB's cytoplasmic domain secondary structure will be an important factor in understanding PLB−SERCA binding.

Alternative Interpretations. Although our dynamics and accessibility data, taken together with other data cited above (*17*, *49*), support the model in Figure 12, further work is needed to rule out alternative models. For example, it is likely that the spin label motions observed in this study are influenced by motions of the probe relative to the protein backbone, which might exaggerate the actual protein dynamics that are present and affect conclusions about multiple components. However, recent EPR studies (to be published separately) with a spin label rigidly coupled to the peptide backbone show even more clearly the presence of two conformational components. It is possible that the observed pattern of mobility and accessibility changes is due primarily to structural changes in the vicinity of Cys11, without the large-scale conformational change envisioned in Figure 12. This must be tested by the use of probes attached to other sites on PLB, but this effort is complicated by the high sensitivity of PLB's function to mutation and other structural perturbation (*52*).

Future Studies. As discussed above, a more systematic investigation of the dynamic equilibrium between the ordered and disordered states will provide valuable insight into the mechanism of binding of PLB's cytoplasmic domain to SERCA, elucidating the role of helix stability in the inhibitory potency of PLB. In addition, SDSL of other residues in PLB is essential for a complete understanding of the structural changes in PLB between the SERCA-bound and unbound forms, and this work is ongoing in our laboratory. In particular, experiments with doubly labeled PLB should provide a more rigorous test for proposed changes in helix stability. Addition of physiologically important perturbants such as PLB phosphorylation and calcium are also vital for understanding inhibition by PLB. Fortunately, as we have established here, EPR is an efficient and informative technique for elucidating these topics. In addition to providing more detailed information about PLB's interaction with SERCA, these studies may also suggest

targets for disruption of inhibition of SERCA by PLB, which could lead to therapies for treating heart disease that arises from, or leads to, pathological calcium handling in cardiac muscle.

ACKNOWLEDGMENT

We thank Zhiwen Zhang for excellent technical assistance in preparing PLB peptides, Leeann Higgins for assistance in the Facility for Mass Spectrometry in the Life Sciences (University of Minnesota), John Stamm for helpful discussion during the early phase of this research, and Yuri Nesmelov for advice concerning the computational analysis of spin label dynamics. We thank Jinny Johnson and Dr. Lawrence Dangott for assistance with amino acid analysis at the Protein Chemistry Laboratory, Texas A&M University.

REFERENCES

1. MacLennan, D. H., Rice, W. J., and Green, N. M. (1997) The mechanism of Ca^{2+} transport by sarco(endo)plasmic reticulum Ca^{2+}-ATPases, *J. Biol. Chem. 272*, 28815−28818.
2. Simmerman, H. K., and Jones, L. R. (1998) Phospholamban: protein structure, mechanism of action, and role in cardiac function, *Physiol. Rev. 78*, 921−947.
3. Katz, A. M., Tada, M., and Kirchberger, M. A. (1975) Control of calcium transport in the myocardium by the cyclic AMP−Protein kinase system, *Adv. Cyclic Nucleotide Res. 5*, 453−472.
4. Bilezikjian, L. M., Kranias, E. G., Potter, J. D., and Schwartz, A. (1981) Studies on phosphorylation of canine cardiac sarcoplasmic reticulum by calmodulin-dependent protein kinase, *Circ. Res. 49*, 1356−1362.
5. Fujii, J., Ueno, A., Kitano, K., Tanaka, S., Kadoma, M., and Tada, M. (1987) Complete complementary DNA-derived amino acid sequence of canine cardiac phospholamban, *J. Clin. Invest. 79*, 301−304.
6. Inui, M., Kadoma, M., and Tada, M. (1985) Purification and characterization of phospholamban from canine cardiac sarcoplasmic reticulum, *J. Biol. Chem. 260*, 3708−3715.
7. Simmerman, H. K., Collins, J. H., Theibert, J. L., Wegener, A. D., and Jones, L. R. (1986) Sequence analysis of phospholamban. Identification of phosphorylation sites and two major structural domains, *J. Biol. Chem. 261*, 13333−13341.
8. Wegener, A. D., Simmerman, H. K., Liepnieks, J., and Jones, L. R. (1986) Proteolytic cleavage of phospholamban purified from canine cardiac sarcoplasmic reticulum vesicles. Generation of a low resolution model of phospholamban structure, *J. Biol. Chem. 261*, 5154−5159.
9. Simmerman, H. K., Lovelace, D. E., and Jones, L. R. (1989) Secondary structure of detergent-solubilized phospholamban, a phosphorylatable, oligomeric protein of cardiac sarcoplasmic reticulum, *Biochim. Biophys. Acta 997*, 322−329.
10. Tatulian, S. A., Jones, L. R., Reddy, L. G., Stokes, D. L., and Tamm, L. K. (1995) Secondary structure and orientation of phospholamban reconstituted in supported bilayers from polarized attenuated total reflection FTIR spectroscopy, *Biochemistry 34*, 4448−4456.
11. Hubbard, J. A., MacLachlan, L. K., Meenan, E., Salter, C. J., Reid, D. G., Lahouratate, P., Humphries, J., Stevens, N., Bell, D., Neville, W. A., *et al.* (1994) Conformation of the cytoplasmic domain of phospholamban by NMR and CD, *Mol. Membr. Biol. 11*, 263−269.
12. Mortishire-Smith, R. J., Pitzenberger, S. M., Burke, C. J., Middaugh, C. R., Garsky, V. M., and Johnson, R. G. (1995) Solution structure of the cytoplasmic domain of phopholamban: phosphorylation leads to a local perturbation in secondary structure, *Biochemistry 34*, 7603−7613.
13. Lockwood, N. A., Tu, R. S., Zhang, Z., Tirrell, M. V., Thomas, D. D., and Karim, C. B. (2003) Structure and function of integral membrane protein domains resolved by peptide-amphiphiles: application to phospholamban, *Biopolymers 69*, 283−292.
14. Mortishire-Smith, R. J., Broughton, H., Garsky, V. M., Mayer, E. J., and Johnson, R. G., Jr. (1998) Structural studies on phospholamban and implications for regulation of the Ca^{2+}-ATPase, *Ann. N.Y. Acad. Sci. 853*, 63−78.
15. Pollesello, P., Annila, A., and Ovaska, M. (1999) Structure of the 1−36 amino-terminal fragment of human phospholamban by nuclear magnetic resonance and modeling of the phospholamban pentamer, *Biophys. J. 76*, 1784−1795.
16. Lamberth, S. H., Schmidt, M., Muenchbach, M., Vorherr, T., Krebs, J., Carafoli, E., and Griesinger C. (2000) NMR solution structure of phospholamban, *Helv. Chim. Acta 83*, 2141−2152.
17. Zamoon, J., Mascioni, A., Thomas, D. D., and Veglia, G. (2003) NMR Solution Structure and Topological Orientation of Monomeric Phospholamban in Dodecylphosphocholine Micelles, *Biophys. J. 85*, 2589−2598.
18. Mascioni, A., Karim, C., Zamoon, J., Thomas, D. D., and Veglia, G. (2002) Solid-state NMR and rigid body molecular dynamics to determine domain orientations of monomeric phospholamban, *J. Am. Chem. Soc. 124*, 9392−9393.
19. Reddy, L. G., Jones, L. R., Cala, S. E., O'Brian, J. J., Tatulian, S. A., and Stokes, D. L. (1995) Functional reconstitution of recombinant phospholamban with rabbit skeletal Ca^{2+}-ATPase, *J. Biol. Chem. 270*, 9390−9397.
20. Kimura, Y., Kurzydlowski, K., Tada, M., and MacLennan, D. H. (1996) Phospholamban regulates the Ca^{2+}-ATPase through intramembrane interactions, *J. Biol. Chem. 271*, 21726−21731.
21. Kimura, Y., Asahi, M., Kurzydlowski, K., Tada, M., and MacLennan, D. H. (1998) Phospholamban domain I/cytochrome b5 transmembrane sequence chimeras do not inhibit SERCA2a, *FEBS Lett. 425*, 509−512.
22. Toyofuku, T., Kurzydlowski, K., Tada, M., and MacLennan, D. H. (1994) Amino acids Glu2 to Ile18 in the cytoplasmic domain of phospholamban are essential for functional association with the Ca^{2+}-ATPase of sarcoplasmic reticulum, *J. Biol. Chem. 269*, 3088−3094.
23. Kimura, Y., Asahi, M., Kurzydlowski, K., Tada, M., and MacLennan, D. H. (1998) Phospholamban domain Ib mutations influence functional interactions with the Ca^{2+}-ATPase isoform of cardiac sarcoplasmic reticulum, *J. Biol. Chem. 273*, 14238−14241.
24. Toyoshima, C., Asahi, M., Sugita, Y., Khanna, R., Tsuda, T., and MacLennan, D. H. (2003) Modeling of the inhibitory interaction of phospholamban with the Ca^{2+} ATPase, *Proc. Natl. Acad. Sci. U.S.A. 100*, 467−472.
25. Hutter, M. C., Krebs, J., Meiler, J., Griesinger, C., Carafoli, E., and Helms, V. (2002) A structural model of the complex formed by phospholamban and the calcium pump of sarcoplasmic reticulum obtained by molecular mechanics, *ChemBioChem 3*, 1200−1208.
26. Toyofuku, T., Kurzydlowski, K., Tada, M., and MacLennan, D. H. (1994) Amino acids Lys-Asp-Asp-Lys-Pro-Val402 in the Ca^{2+}-ATPase of cardiac sarcoplasmic reticulum are critical for functional association with phospholamban, *J. Biol. Chem. 269*, 22929−22932.
27. Jones, L. R., Cornea, R. L., and Chen, Z. (2002) Close proximity between residue 30 of phospholamban and cysteine 318 of the cardiac Ca^{2+} pump revealed by intermolecular thiol cross-linking, *J. Biol. Chem. 277*, 28319−28329.
28. Young, H. S., Jones, L. R., and Stokes, D. L. (2001) Locating phospholamban in co-crystals with Ca^{2+}-ATPase by cryoelectron microscopy, *Biophys. J. 81*, 884−894.
29. Toyoshima, C., and Nomura, H. (2002) Structural changes in the calcium pump accompanying the dissociation of calcium, *Nature 418*, 605−611.
30. Fujii, J., Maruyama, K., Tada, M., and MacLennan, D. H. (1989) Expression and site-specific mutagenesis of phospholamban. Studies of residues involved in phosphorylation and pentamer formation, *J. Biol. Chem. 264*, 12950−12955.
31. Karim, C. B., Marquardt, C. G., Stamm, J. D., Barany, G., and Thomas, D. D. (2000) Synthetic null-cysteine phospholamban analogue and the corresponding transmembrane domain inhibit the Ca-ATPase, *Biochemistry 39*, 10892−10897.
32. Fernandez, J. L., Rosemblatt, M., and Hidalgo, C. (1980) Highly purified sarcoplasmic reticulum vesicles are devoid of Ca^{2+}-independent ('basal') ATPase activity, *Biochim. Biophys. Acta 599*, 552−568.
33. Stokes, D. L., and Green, N. M. (1990) Three-dimensional crystals of CaATPase from sarcoplasmic reticulum. Symmetry and molecular packing, *Biophys. J. 57*, 1−14.
34. Reddy, L. G., Autry, J. M., Jones, L. R., and Thomas, D. D. (1999) Co-reconstitution of phospholamban mutants with the Ca-ATPase reveals dependence of inhibitory function on phospholamban structure, *J. Biol. Chem. 274*, 7649−5765.

35. Reddy, L. G., Cornea, R. L., Winters, D. L., McKenna, E., and Thomas, D. D. (2003) Defining the molecular components of calcium transport regulation in a reconstituted membrane system, *Biochemistry 42*, 4585−4592.
36. Madden, T. D., Chapman, D., and Quinn, P. J. (1979) Cholesterol modulates activity of calcium-dependent ATPase of the sarcoplasmic reticulum, *Nature 279*, 538−541.
37. Karim, C. B., Paterlini, M. G., Reddy, L. G., Hunter, G. W., Barany, G., and Thomas, D. D. (2001) Role of cysteine residues in structural stability and function of a transmembrane helix bundle, *J. Biol. Chem. 274* (42), 38814−38819.
38. Columbus, L., and Hubbell, W. L. (2002) A new spin on protein dynamics, *Trends Biochem. Sci. 27*, 288−295.
39. Budil, D. E., Lee, S., Saxena, S., and Freed, J. H. (1996) Nonlinear-Least-Squares Analysis of Slow-Motion EPR Spectra in One and Two Dimensions Using a Modified Levenberg−Marquardt Algorithm, *J. Magn. Reson., Ser. A 120*, 155−189.
40. Altenbach, C., Greenhalgh, D. A., Khorana, H. G., and Hubbell, W. L. (1994) A collision gradient method to determine the immersion depth of nitroxides in lipid bilayers: application to spin-labeled mutants of bacteriorhodopsin, *Proc. Natl. Acad. Sci. U.S.A. 91*, 1667−1671.
41. Pali, T., and Marsh, D. (2002) Structural studies on membrane proteins using non-linear spin label EPR spectroscopy, *Cell. Mol. Biol. Lett. 7*, 87−91.
42. Farahbakhsh, Z. T., Altenbach, C., and Hubbell, W. L. (1992) Spin labeled cysteines as sensors for protein−lipid interaction and conformation in rhodopsin, *Photochem. Photobiol. 56*, 1019−1033.
43. Cornea, R. L., Jones, L. R., Autry, J. M., and Thomas, D. D. (1997) Mutation and phosphorylation change the oligomeric structure of phospholamban in lipid bilayers, *Biochemistry 36*, 2960−2967.
44. Li, M., Reddy, L. G., Bennett, R., Silva, N. D., Jr., Jones, L. R., and Thomas, D. D. (1999) A fluorescence energy transfer method for analyzing protein oligomeric structure: application to phospholamban, *Biophys. J. 76*, 2587−2599.
45. Columbus, L., Kalai, T., Jeko, J., Hideg, K., and Hubbell, W. L. (2001) Molecular motion of spin labeled side chains in α-helices: analysis by variation of side chain structure, *Biochemistry 40*, 3828−3846.
46. Gross, A., and Hubbell, W. L. (2002) Identification of protein side chains near the membrane-aqueous interface: a site-directed spin labeling study of KcsA, *Biochemistry 41*, 1123−1128.
47. Karim, C. B., Stamm, J. D., Karim, J., Jones, L. R., and Thomas, D. D. (1998) Cysteine reactivity and oligomeric structures of phospholamban and its mutants, *Biochemistry 37*, 12074−12081.
48. Hubbell, W. L., Cafiso, D. S., and Altenbach, C. (2000) Identifying conformational changes with site-directed spin labeling, *Nat. Struct. Biol. 7*, 735−739.
49. Negash, S., Yao, Q., Sun, H., Li, J., Bigelow, D. J., and Squier, T. C. (2000) Phospholamban remains associated with the Ca^{2+}- and Mg^{2+}-dependent ATPase following phosphorylation by cAMP-dependent protein kinase, *Biochem. J. 351*, 195−205.
50. Chen, B., and Bigelow, D. J. (2002) Phosphorylation induces a conformational transition near the lipid-water interface of phospholamban reconstituted with the Ca-ATPase, *Biochemistry 41*, 13965−13972.
51. Hughes, E., and Middleton, D. A. (2003) Solid-state NMR reveals structural changes in phospholamban accompanying the functional regulation of Ca^{2+}-ATPase, *J. Biol. Chem. 278* (23), 20835−20842.
52. MacLennan, D. H., and Kranias, E. G. (2003) Phospholamban: a crucial regulator of cardiac contractility, *Nat. Rev. Mol. Cell. Biol. 4*, 566−577.

BI035749B